Journal of ELECTRONIC MATERIALS, Vol. 49, No. 5, 2020
https://doi.org/10.1007/s11664-020-08018-9


# Quasi-3D Perfect Absorber Based on the Self-Similar Parasitic Elements as an Optical Sensor with Tunable Attributes for Near-Infrared Application

FATEMEH TAVAKOLI [1] and R.A. SADEGHZADEH[2,3]

1.—Faculty of Engineering, Science and Research Branch, Islamic Azad University, Tehran, Iran.
2.—Faculty of Electrical Engineering, K. N. Toosi University of Technology, Tehran, Iran.
3.—e-mail: sadeghz@eetd.kntu.ac.ir

We have designed a novel self-similar plasmonic perfect absorber with a quasi-three-dimensional (3D) shape based on parasitic elements, which is useful as a refractive index sensor for near-infrared applications. In order to achieve tunable attributes, we have applied the liquid crystal medium to provide a tunable structure which can be considered to control the absorption parameter and resonances. In fact, we have proposed a self-similar structure to obtain a multi-band structure in the range of 800–1600 nm with an absorption value up to 99.8%. The basic model is a single cross element, while each quarter is filled up by L-shaped elements by forming a tapered shape like a pyramidal in which the elements are arranged from large to small with various heights and lengths which creates a ziggurat form. So this structure can provide a quad-band absorber which we have implemented as a refractive index sensor with a much higher figure of merit (FOM) in comparison to the flat formations. For the final structure, the maximum values of the FOM and sensitivity ($S$) are 24,560 $RIU^{-1}$ and 660 nm $RIU^{-1}$, respectively.

**Key words:** Absorber, plasmonic, near-infrared, liquid crystal

## INTRODUCTION

Metamaterial (MMA) is known as a periodic or non-periodic artificial structure, with unique properties that are not found in nature.[1] Plasmonic metamaterials (MMAs) are usually contained noble metals so that the individual dimensions are smaller than the operating wavelength.[2] So, due to their forms, they have different values of permeability and permittivity.[3] Thus, they show different performance such as negative permittivity and permeability.[4,5] By some change in their shapes and manipulating electromagnetic waves, it is possible to obtain different characteristics such as negative refraction or perfect absorption.[6–8] Because of these features, the metamaterials (MMAs) can be used in applications such as solar cells,[9] near-field scanning optical microscopy (NSOM),[10] surface-enhanced Raman scattering (SERS),[11] and biological applications.[12]

Surface plasmon resonance (SPR) in nanostructures smaller than light wavelengths is called the localized surface plasmons resonance (LSPR). Surface plasmon polaritons (SPPs) are made by electromagnetic excitation which can be propagated at the metal and dielectric interface.[13] They are important because of their ability to concentrate electromagnetic fields and reduce their dispersion in optical frequencies, which causes the development of localized fields several times large.[14] The plasma frequency of the free electron gas can be obtained by $\omega_p^2 = ne^2/\varepsilon_0 m$, where $n$ is the number density of free electron gas, $\varepsilon_0$ is the air dielectric constant, and $m$ is the effective optical mass of each electron. At frequencies much larger than the collision frequency $\gamma$, the permittivity is approximately $\varepsilon(\omega) =$

(Received September 3, 2019; accepted February 12, 2020; published online February 21, 2020)

$1-\omega_p^2/\omega^2$ and for frequencies smaller than the plasma frequency, the permittivity has a negative value and provides the propagation of plasmonic waves.[15] Because of the resonance frequency sensitivity to the refractive index of the surrounding environment, changing the refractive index of the environment shifts the resonance frequency, which provides the possibility for use in nano-sensor applications.[16]

Plasmonic absorbers and antennas have been considered for various applications such as optical sensing as refractive index sensors, with compact size and high figure of merit (FOM) with single resonance[17] for detecting materials such as antigens, and also in the optical domain with multi-resonance.[18] On the other hand, the optical metal-insulator-metal (MIM) couple line has been suggested for higher accuracy because of its higher figure of merit (FOM);[19] however, the fabrication of the metal-insulator-metal (MIM) line is a challenge, and absorbers with high figure of merit (FOM) are more desirable. In addition, some noble metals such as gold and silver are considered the best plasmonic materials due to the ability to stimulate plasmons.[20]

Previous studies on three-dimensional (3D) structures have been reported.[21,22] For example, in,[21] a plasmonic hollow cylindrical absorber is proposed and can be manufactured with new technologies, in which the influence of the cylinder height on the quality factor ($Q$-factor), and thus the absorption rate is investigated. Also, in,[22] a three-dimensional (3D) metamaterial absorber is presented which is applicable in an ultra-broadband frequency range.

In this paper, we have designed a quasi-three-dimensional (3D) perfect absorber based on a novel structure of self-similar and symmetrical formation that is suitable for TE or TM mode. In fact, we have applied the parasitic elements between the unit cells to control the absorption and number of resonances by considering the effect of the gap between the elements on the capacitors of the equivalent circuit[23] Furthermore, we have improved the absorption rate by designing a quasi-three-dimensional (3D) nanostructure and examining the effect of the height of the fractal elements.

On the other hand, we have implemented the liquid crystal (LC) as a substrate to design a tunable structure and the liquid crystal (LC) molecules can be adjusted by an external electric field.[24] We have calculated the figure of merit (FOM) and sensitivity ($S$) of the sensor of the final model. As a matter of fact, we have provided a perfect absorber which can be useful for optical sensing with higher quality. We have obtained the figure of merit (FOM) about 24000 $RIU^{-1}$ and this is a high value more than the metal-insulator-metal (MIM) refractive index sensors.

## ABSORBER DESIGNING AND MODELING

In this proposed perfect absorber, we have used silver as a plasmonic material, so that using the Drude model, the permittivity is expressed as shown in Eq. 1:[25]

$$\varepsilon(\omega)=\varepsilon_\infty-\frac{\omega_p^2}{\omega^2+i\gamma\omega} \tag{1}$$

where $\omega_p$ is the plasma frequency, $\varepsilon_\infty$ is the dielectric constant (usually $1<\varepsilon_\infty<10$), $\omega$ is the operating frequency of incident light and $\tau=1/\gamma$ is the relaxation time and $\gamma$ is collision frequency,[25] so that $\omega_p=1.39\times10^{16}$ Hz, $\varepsilon_\infty=3.7$, and $\tau=3.1\times10^{-14}$ s.

Figure 1 shows the geometry and designing steps as a perfect absorber with ziggurat form. There is a dielectric layer of aluminum oxide ($Al_2O_3$) with a refractive index of 1.75 and thickness and the length of $H_d=45$ nm and $L_d=770$ nm, respectively, located between two silver layers. The specification of the silver metal is in accordance with the data measured in the experiments of Johnson and Christy.[25] The thickness of the bottom silver substrate is assumed to be$H_b=80$ nm which is larger than the skin depth[26] and avoids any transmittance. The designing is done in four steps. At first, a cross element is examined with the thickness and the length of $H_c=70$ nm and $L_c=660$ nm, respectively. Then, each of the L-shaped parasitic elements with various heights and lengths are added to the structure, while in the first step, the height, the width and the length of the L-shaped element is $H_1=60$ nm, $W_1=20$ nm, and $L_1=285$ nm, respectively, and the gap with the cross is $g_1=10$ nm, for the second step, the height, the width and the length of the L-shaped element is assumed $H_2=50$ nm, $W_2=20$ nm, and $L_2=220$ nm, respectively, and the gap with the previous L-shaped element is $g_2=15$ nm. In the last step, in which the ziggurat form is completed, the height, the width and the length of the L-shaped element is $H_3=45$ nm, $W_3=20$ nm, and $L_3=145$ nm, respectively, and the gap with the previous L-shaped element is $g_3=15$ nm. Recently, nano-antenna with a gap size of 7.5 nm is designed and fabricated. It means 10 nm gaps are possible for fabrication and we consider for our simulation.[27]

In the next step, we have replaced the dielectric layer with a liquid crystal (LC) medium to create a tunable structure. Liquid crystal (LC) materials have properties that are a combination of a crystalline solid and a conventional liquid and show specific symmetries, depending on the orientation and rotation angles of their molecules. In a nematic liquid crystal (LC) which is an anisotropic medium,[28] the positions of molecules have a discrete rotational symmetry but similar orientation. In

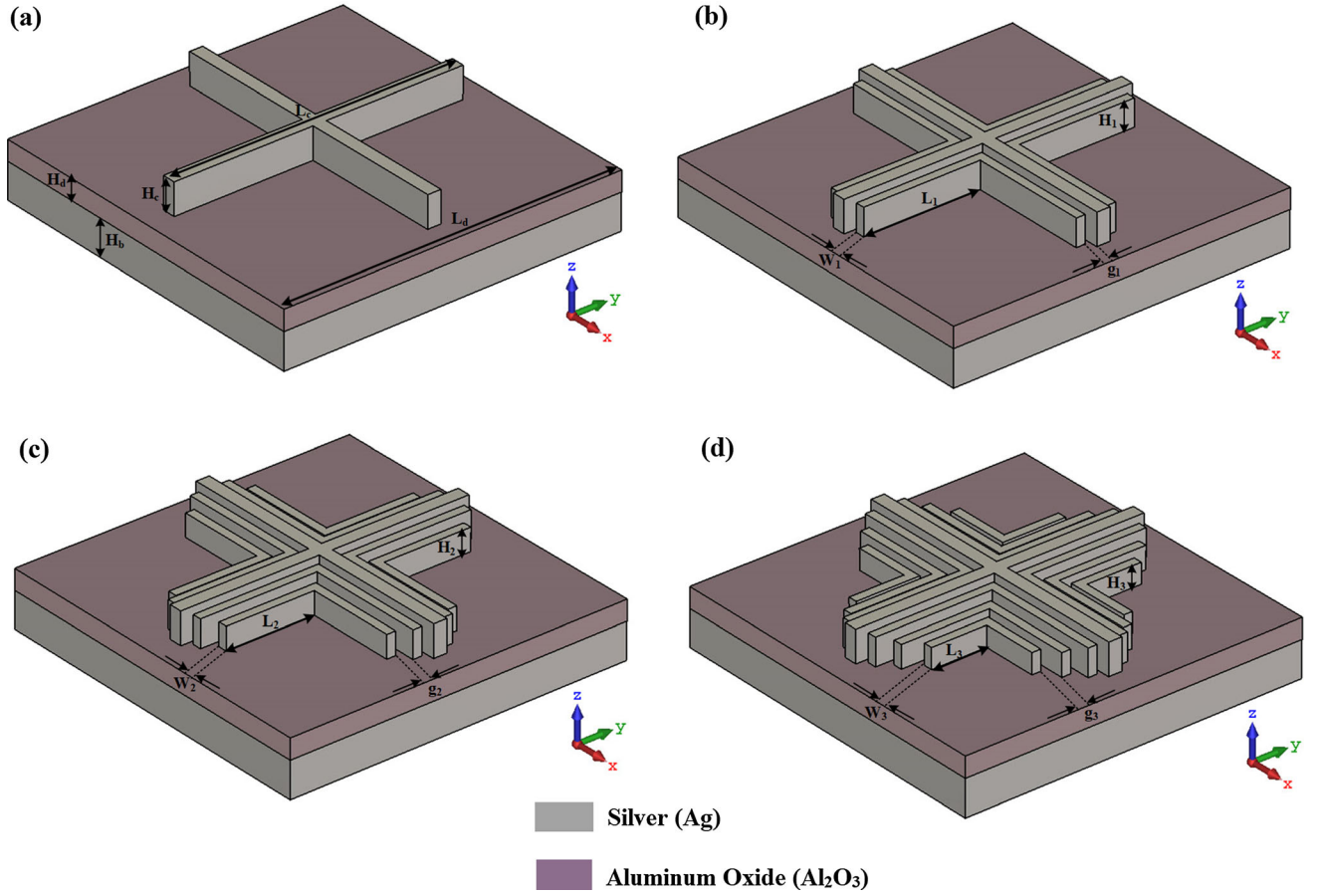


Fig. 1. The geometry and designing steps for perfect absorber with ziggurat form. (a) the single cross element (b) adding the first parasitic L-shape element (c) adding the second parasitic L-shape element (d) adding the third parasitic L-shape element while the all dimensions are $H_d = 45$ nm, $L_d = 770$ nm, $H_b = 80$ nm, $H_c = 70$ nm, $L_c = 660$ nm, $H_1 = 60$ nm, $W_1 = 20$ nm, $L_1 = 285$ nm, $g_1 = 10$ nm, $H_2 = 50$ nm, $W_2 = 20$ nm and $L_2 = 220$ nm, $g_2 = 15$ nm, $H_3 = 45$ nm, $W_3 = 20$ nm, $L_3 = 145$ nm, $g_3 = 15$ nm

addition, its permittivity is described by a second rank tensor and we have assumed that $\varepsilon_o = 3$ and $\varepsilon_e = 4$ are ordinary and extraordinary permittivity, respectively.[28]

In order to analyze the proposed perfect absorber, under a TE-mode plane-wave light source in $z$-axis injection and backward direction, we have used commercial software (Lumerical FDTD Solutions) that utilizes a three-dimensional (3D) finite-difference time-domain (FDTD) method.[29] In order for the parameter settings to be based on the finite-difference time-domain (FDTD), which is a numerical method for solving Maxwell's equations and exploiting Fourier transforms for calculating the complex Poynting vector and the transmission or reflection of light, we have applied periodic boundary conditions on the $x$- and $y$-axis and perfectly matched layers (PMLs) on the $z$-axis for absorbing optical waves and minimizing reflection with 32 layers in order to confirm the stability of our simulations. Also, we have placed tow frequency-domain power monitors above the plane-wave source and bottom of the structure to calculating the reflected and transmitted waves, respectively. Furthermore, the illumination bandwidth range is considered in the near-infrared region and is 800 nm to 1600 nm.

## ABSORBER SIMULATION RESULTS AND DISCUSSION

### Designing the Quasi-3D Absorber in the Ziggurat Form

As shown in Fig. 2, we have checked the absorption value for all four steps of design and the results are presented. Since the transmission value is almost zero due to the presence of the bottom metal substrate and small value of the skin depth at this frequency range,[30] the absorption value ($A$) is obtained as $A = 1 - R - T = 1 - R$,[31,32] where $R$ and $T$ are the reflection and transmission values, respectively.[33] In absorber structures, the cross or any nanoparticles can be considered the central nucleus. However, due to the structural simplicity of the composite structure of cut wires, we can extend the absorber to a more symmetric structure by replacing with crosses, so high absorption can be obtained in this more symmetric composite structure for both TE and TM polarizations.[34]

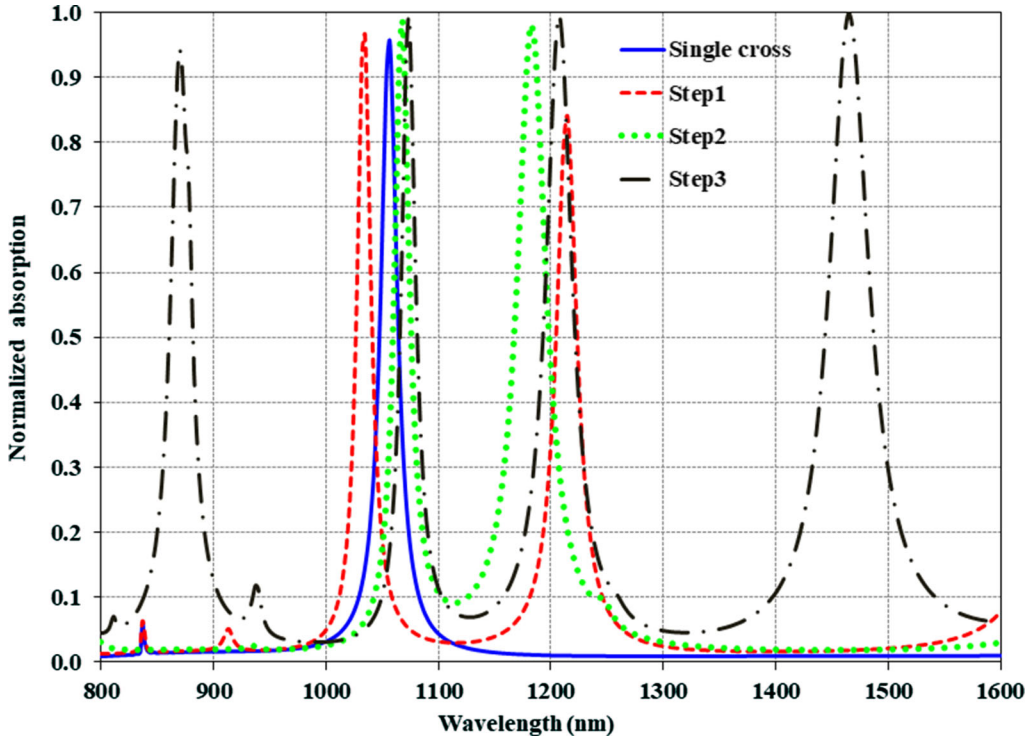


Fig. 2. The normalized absorption for all four steps of designing the ziggurat form

On the other hand, according to recent research, capacitors between unit cells and adjacent elements with the main elements are an efficient way to control resonance frequency and absorption value. Also, simple structures in sensor applications have problems such as low sensitivity ($S$). Furthermore, anisotropic nanoparticles make the structure sensitive to polarization and incident angle which is one of the most fundamental problems in manufacturing these structures. Thus, by applying symmetric nanoparticles as parasitic elements, we can design polarization-independent structures. Moreover, we can control the capacitor between adjacent elements with the main element and create a new resonant circuit.[23] So, in addition to maintaining the main resonant frequency, we can add new resonances, thereby increasing sensitivity and the figure of merit (FOM). As it is obvious here, by increasing the number of parasitic elements, the absorption values increased drastically while we can obtain a perfect absorber. In addition, by using fractal nanoparticles, we can produce multi-band responses and tune optical properties. Fractals are the fragmented geometric shape that can be repeated sequentially on smaller scales so that each part is a reduced-size copy of the whole. Because of the multiscale and self-similarity properties of fractals, we can obtain multiple-band spectral responses which by increasing the fractal order, the optical resonances can increase.[35,36]

On the other hand, we have used the quasi-three-dimensional (3D) shape as a method to enhance absorption[37] for all resonances. As the basic model, we have investigated a single cross element that has only a resonance peak at the wavelength of 1056 nm and the absorption is about 95%. In fact, the resonant frequency of the absorber can be expressed by the inductance and capacitance of the equivalent circuit. Whereas for the basic model, the inductance is due to the metal cross element and the capacitance is due to the gap between the unit cells, which depends on the width and size of the gap. So the resonance frequency can be obtained from $f = 1/2\pi\sqrt{LC}$.[23]

In the first step, by adding an L-shaped element in each quarter, two resonances are obtained at 1034 nm and 1214 nm with absorption of 96% and 78%, respectively, while the second absorption is not attractive for us. In the second step, we have added another L-shaped element with a smaller length and height, and two resonances are obtained at 1068 nm and 1182 nm with higher absorption of 99% and 98%, respectively. Hence, as shown herein, we can modify the resonances by making a trap and concentrating the energy. In the last step, we have improved the resonance number by adding another L-shaped element and providing a ziggurat form. In addition, it can provide a quad-band absorber with absorbance of 94%, 99% at wavelengths of 869 nm and 1073 nm, respectively, and the absorbance is more than 99% at wavelengths of 1207 nm and 1464 nm, which can improve the quality of sensitivity ($S$). Therefore, it is expected that our proposed structure will be applicable in many devices such as optical sensors.

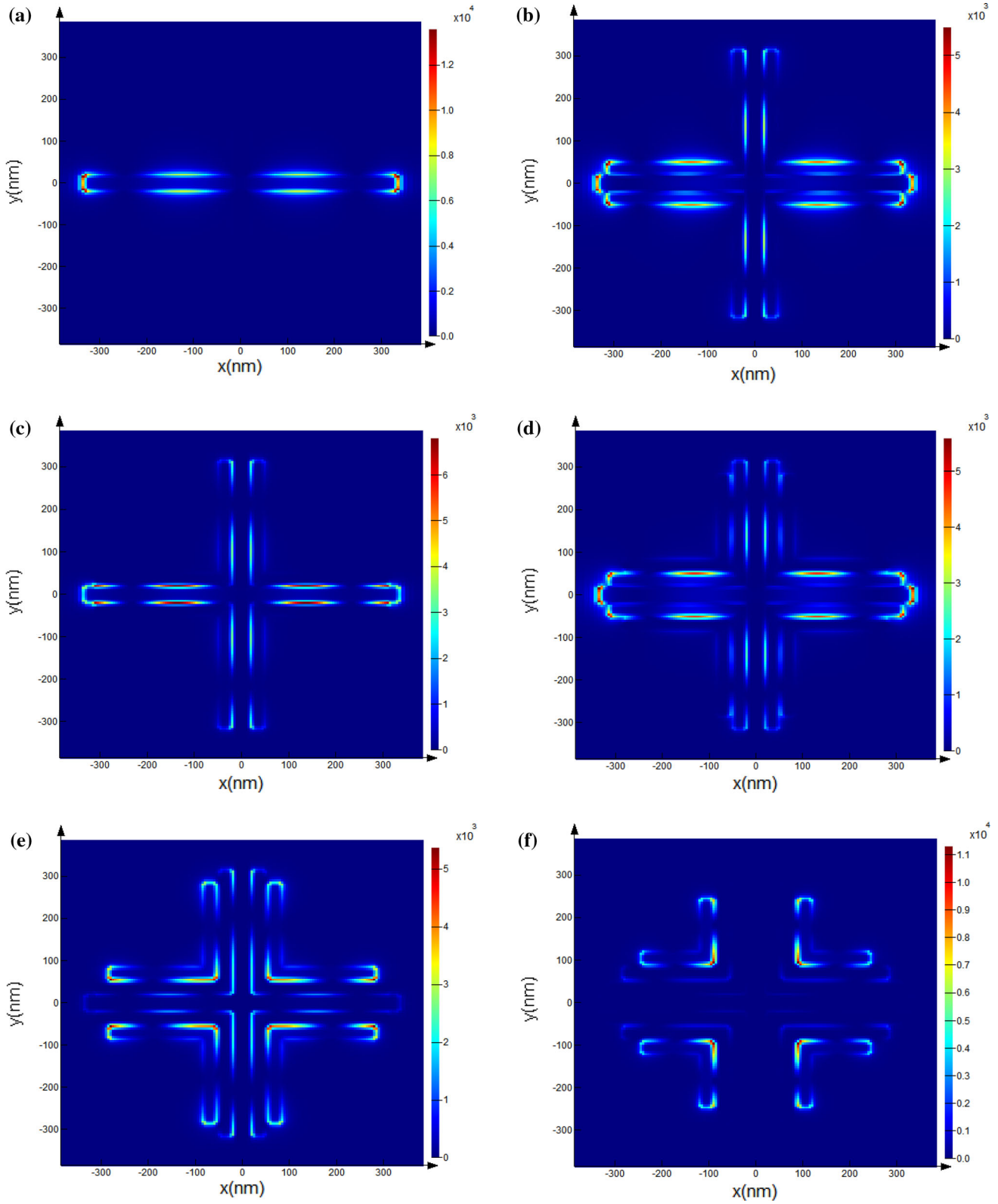


Fig. 3. The electric field intensity and distribution for all four steps of design of the ziggurat form at the resonance wavelengths (a) for the single cross at 1056 nm; for the first parasitic L-shaped element in (b) 1034 nm and (c) 1214 nm; for the second parasitic L-shaped element in (d) 1068 nm and (e) 1182 nm; for the third parasitic L-shaped element in (f) 869 nm, (g) 1073 nm, (h) 1207 nm and (i) 1464 nm

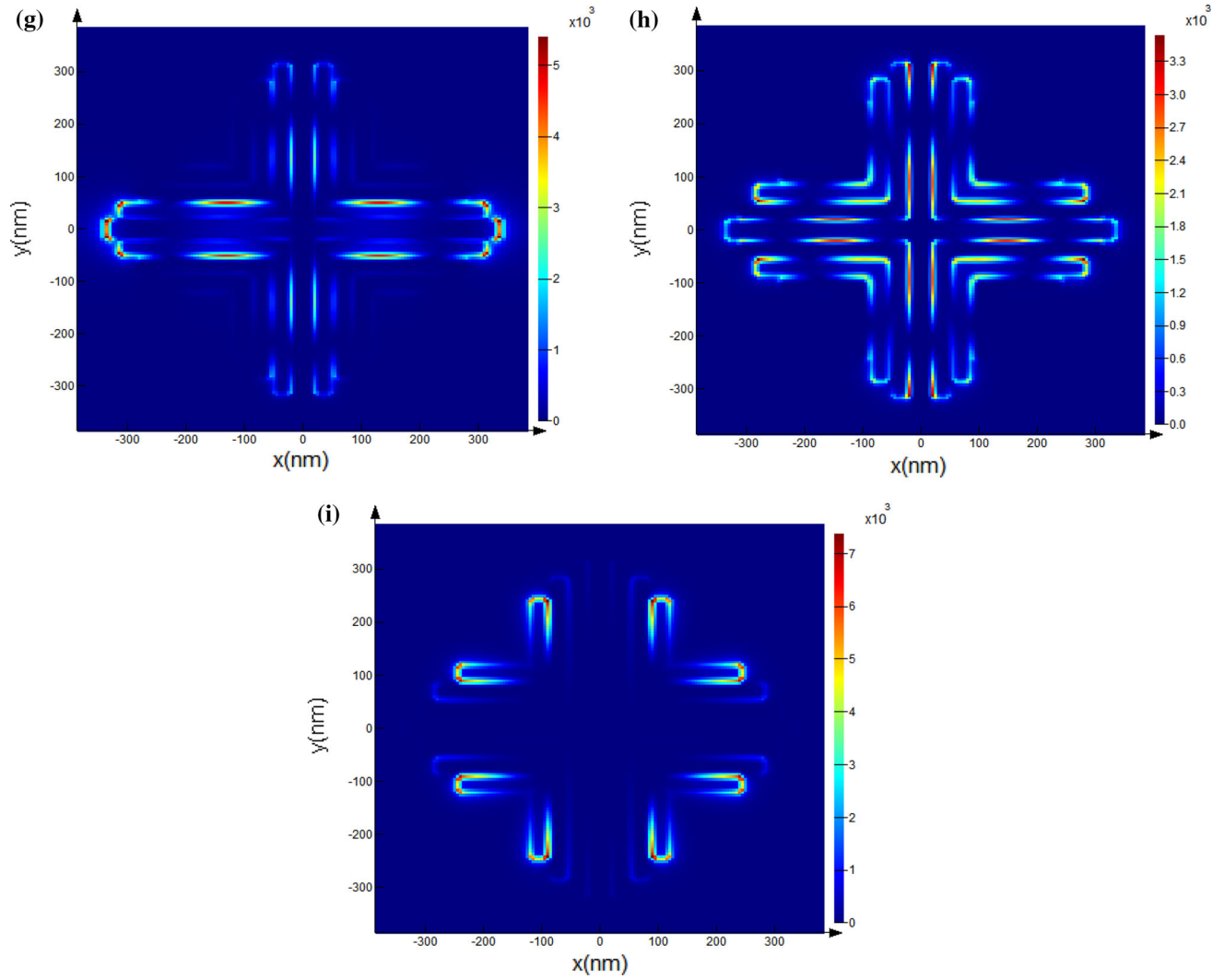


Fig. 3. continued

The electric field distribution is presented for all studied cases in Fig. 3. According to Fig. 3a, we can say that for a single cross, the electric field is distributed only along the horizontal strip with the maximum intensity of $1.4 \times 10^4$. Therefore, as shown in Fig. 2, we do not have more than one resonance at 1056 nm. In order to achieve more resonance, we have added symmetric parasitic elements with the L-shaped form to our proposed structure. Generally, we follow the two main goals. First, it can maintain the symmetry of the structure and the incident wave polarization does not have an impact on the structure. Second, we can create new resonances and multi-band properties into the proposed structure.

As shown in Fig. 3b and c, in the first step, the field is distributed both in the parasitic elements and the main cross. In the first resonance, the electric fields focus on the edges of the rods with maximum value $5.5 \times 10^3$, but in the second resonance, the electric field is dispersed along the horizontal strip of the cross with maximum value $6.8 \times 10^3$. However, we can see that the parasitic elements have some effects on the main cross too. This behavior can be seen also for the next step of design. In fact, adding more parasitic elements can reduce the effect of the main cross more. As exhibited in Fig. 2, in the second step, two resonances appear which are similar to the resonances, as in the first step. So we expect the field behaviors to be similar to the previous one as presented in Fig. 3d. It should be noted, however, that we said that by adding parasitic elements, their effect is reduced by the cross, which can be seen in the second resonance in Fig. 3e.

Finally, in our final structure, the number of resonances reaches four. As presented in Fig. 3f, the first resonance is made by the parasitic elements and there is no coupling between this element and the cross element. But in the second resonance as

presented in Fig. 3g, the effect of the cross and first parasitic elements combination are visible. Of course, we can see this form of distribution of the electric field in the previous structures in Fig. 3b and d. For the third resonance, as shown in Fig. 3h, the greater coupling effect is visible and we expect more absorption for this resonance as we can see in Fig. 2. Finally, as shown in Fig. 3i, the last resonance in higher wavelength is oriented from the third parasitic element.

## Analyzing the Quasi-3D Absorber in the Ziggurat Form

Determined based on the parallel surface or coupling of elements.[38–40] Furthermore, we should note that surface plasmons are formed at the interface of the metal and dielectric. Of course, the plasmons also can be formed at the surface of the metal and air.[41] So, when the height is reduced, the plasmon is distributed at the height. In addition, the capacitance increases and the resonances shift to higher wavelengths, or, in other words, lower frequencies. It is noteworthy that due to the small difference in layer height, which is in total less than $\lambda/4$, the radiation wave at the incidence of the proposed structure acts as a relatively uniform surface. But changes in the capacitor show their behavior as impedance matching.[42]

In order to better understand, we used two tests. In the first analysis, as shown in Fig. 4a, we have considered the whole structure at the same height to the cross element, and this state is called step 1. Then, in step 2, we have considered the height of the cross element at 70 nm and other elements at 60 nm. In step 3, we have assumed the height of the cross is 70 nm while the first parasitic element is 60 nm and other elements are 50 nm. At last, for the final model, we have checked the ziggurat form with different heights.

In step 1, we have four resonances, one with an absorption of 80% at a wavelength of 844 nm and the others with absorbance of about 98% at the other wavelengths of 1079 nm, 1175 nm, and 1393 nm. In step 2, we have four resonances at wavelengths of 851 nm, 1079 nm, 1189 nm, and 1412 nm with absorptions of 84%, 97%, 99%, and 95%, respectively. In step 3, we have four resonances, one with an absorption of 90% at a wavelength of 862 nm and the others with an absorbance of about 99% at the other wavelengths of 1073 nm, 1207 nm, and 1443 nm. In the final model in which the ziggurat form is completed, the resonances are shifted to higher wavelengths with higher absorbances of 94% and 99% at wavelengths of 869 nm and 1073 nm, respectively, and the absorbance is more than 99% at wavelengths of 1207 nm and 1464 nm. In short, we can say the absorption for all resonances is improved drastically. As the results show, with these changes the impedance matching is improved, and accordingly, the quality of the ziggurat form is better than the other cases. The more important point is that the resonances are shifted to higher wavelengths.

Results from the second analysis are presented in Fig. 4b. In order to verify the effect of the height of each element, we have set the height of the elements similar to every element, with heights of 70 nm, 60 nm, 50 nm, and 45 nm. At first, we have assumed the height of elements is 70 nm, and four resonances have been obtained, the first with an absorption of 80% at a wavelength of 844 nm, with an absorbance of about 98% at wavelengths of 1079 nm and 1175 nm, and an absorbance of 90% at a wavelength of 1393 nm. Then, the heights were changed to 60 nm, and in this case, we have four resonances, one with an absorption of 83% at a wavelength of 853 nm, an absorption of about 99% at wavelengths of 1076 nm and 1192 nm, and an absorbance of 94% at a wavelength of 1412 nm. When the height of all elements is 50 nm, we have four resonances at wavelengths of 864 nm, 1076 nm, 1214 nm, and 1443 nm with absorptions of 87%, 98%, 99%, and 97%, respectively. Finally, the height of all elements is assumed to be 45 nm, and we can see four resonances: with absorptions of 88% and 96% at wavelengths of 871 nm and 1079 nm, respectively, and an absorption of 98% at the other wavelengths of 1229 nm and 1464 nm.

In brief, we have used and discussed the fractal parasitic elements that are placed between the unit cells to construct a new resonance circuit. Also, with the information from the equivalent circuit of the basic structure and the first resonance, we can justify the number of resonances by varying the length and gaps of the fractal parasitic elements, so that the gap capacitances ($C_m$) can be expressed as:[40]

$$C_m = c\varepsilon_0\varepsilon_{\mathrm{d}}\frac{b}{2}\frac{a}{t_{\mathrm{d}}} \tag{2}$$

where $c$ is a constant appropriately chosen to take the fringe effects, $\varepsilon_0$ is the permittivity of free space ($\approx 8.854 \times 10^{-12}$ F m$^{-1}$), $\varepsilon_{\mathrm{d}}$ and $t_{\mathrm{d}}$ are the relative permittivity and thickness of the dielectric spacer, respectively, $a$ and $b$ are the width and length of the top nanostructures. In fact, in the final model, we will have four capacitors and thus four resonances, while by creating gaps between the parasitic elements, in addition to the capacitor caused by the interaction with the bottom plate, more energy is stored in the capacitors due to the coupling effect of gaps. As a result, the absorption rate can increase.

On the other hand, the effect of the height of the elements on the absorption rate and resonance shifts has been investigated. By changing the height of the fractal elements and reduction of the ohmic loss rate, the quality factor ($Q$-factor), and thus the absorption rate, can be increased. Also, resonances shift to higher wavelengths or lower frequencies. So, according to Fig. 4, we can see that the lower height

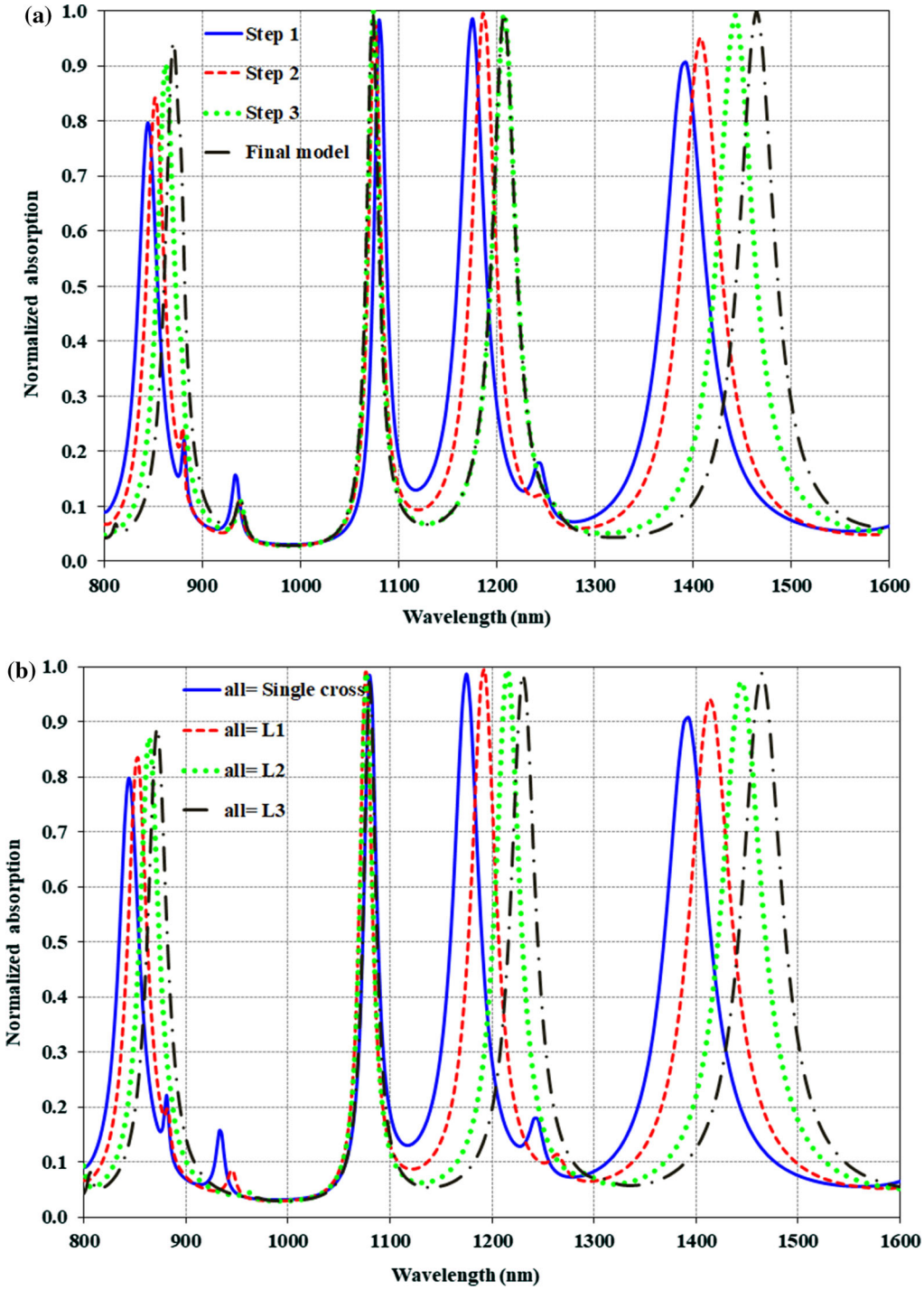


Fig. 4. Analyzing the structure and the normalized absorption for the proposed ziggurat form (a) changing the height of each element, step by step, (b) setting the height of the elements similar to every element with heights of 70, 60, 50, and 45 nm, respectively

is more suitable for improving the absorption. However, the ziggurat form shows better results. Actually, the distributed wave in the ziggurat form provides a surface with suitable impedance for matching and acts like a taper structure the same as a transmission line.

## Designing the Quasi-3D Absorber with Tunable Attributes

There are many materials available in the optics field that have been used as controllers such as organic material[43] graphene[44] and liquid crystal (LC).[45] Since intra-structural methods such as

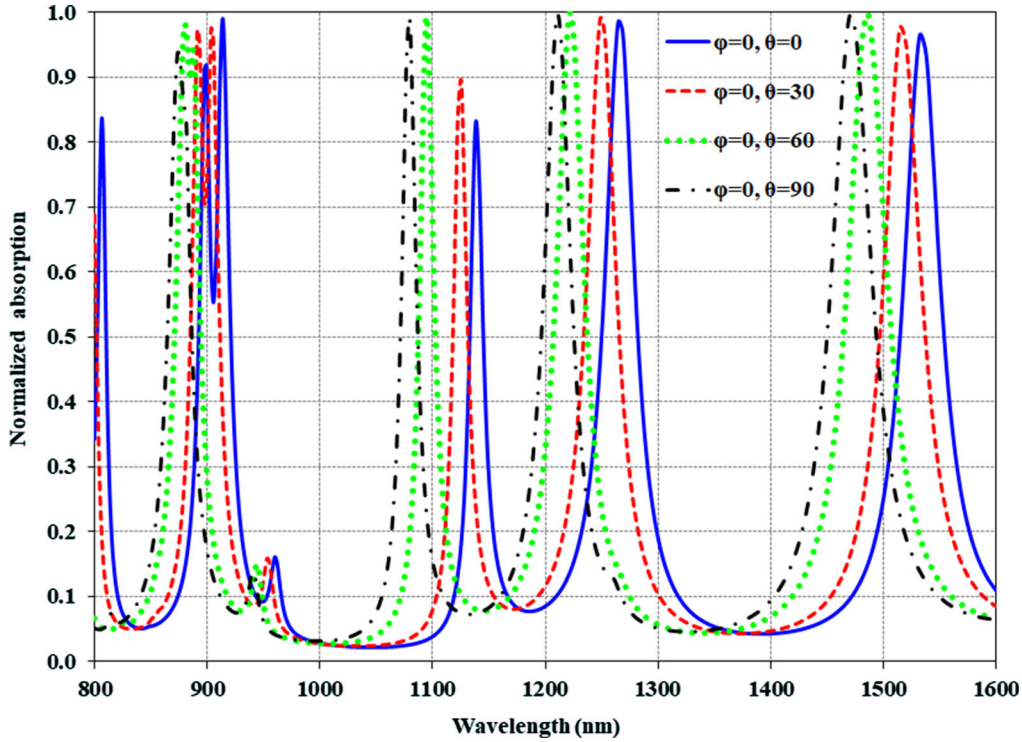


Fig. 5. The normalized absorption for the prototype absorber for the various angle of the liquid crystal (LC)

geometrical changes or properties of materials used in nanostructures to control plasmonic resonance are a static and limited method, the use of liquid crystal is considered a viable option due to the ability to adjust external parameters. Liquid crystal (LC) is a suitable candidate for the development of plasmonic structures, and by adjusting the orientation of the molecules, it provides tunable attributes.[24,28,45] Given the anisotropic optical properties of the liquid crystal (LC) and depending on their orientation, we have defined a transformation matrix as a function of two rotational angles theta and phi with $U(\theta, \varphi)$ as follows in Eqs. 3 and 4:[46]

$$U = U_\varphi \times U_\theta = \begin{bmatrix} \cos\varphi & -\sin\varphi & 0 \\ \sin\varphi & \cos\varphi & 0 \\ 0 & 0 & 1 \end{bmatrix} \times \begin{bmatrix} \cos\theta & 0 & \sin\theta \\ 0 & 1 & 0 \\ -\sin\theta & 0 & \cos\theta \end{bmatrix} \tag{3}$$

$$\varepsilon_{\text{total}} = U \times \varepsilon_{\text{diagonal}} = \begin{bmatrix} \cos\theta\cos\varphi & -\sin\varphi & \sin\theta\cos\varphi \\ \cos\theta\sin\varphi & \cos\varphi & \sin\theta\sin\varphi \\ -\sin\theta & 0 & \cos\theta \end{bmatrix} \times \begin{bmatrix} \varepsilon_\perp & 0 & 0 \\ 0 & \varepsilon_\perp & 0 \\ 0 & 0 & \varepsilon_\parallel \end{bmatrix} = \begin{bmatrix} \varepsilon_{xx} & \varepsilon_{xy} & \varepsilon_{xz} \\ \varepsilon_{yx} & \varepsilon_{yy} & \varepsilon_{yz} \\ \varepsilon_{zx} & \varepsilon_{zy} & \varepsilon_{zz} \end{bmatrix} \tag{4}$$

In the finite-difference time-domain (FDTD) solutions (Lumerical software), to set up an anisotropic material, we have used an appropriate grid attribute object to set the transformation matrix U and we have defined two rotational angles $(\theta, \varphi)$ to specify a spatially varying liquid crystal (LC) director orientation. Also, in the material database, we have defined the permittivity elements as the $\varepsilon_{\text{diagonal}}$. As shown in Eq. 3, if the theta and phi are supposed to be zero then we have only a diagonal matrix with $\varepsilon_{xx}$, $\varepsilon_{yy}$ and $\varepsilon_{zz}$ elements. On the other hand, when we have assumed other value for phi and theta, the other elements of the matrix's entries will not be zero and we have a complicated material when the various elements change from zero to a real value such as $\varepsilon_{xz}$ and $\varepsilon_{zx}$.

Our goal is to show that it is possible to control the resonances by replacing the liquid crystal (LC) medium and specifying a spatially varying liquid crystal (LC) director orientation instead of a normal substrate and also control the resonance by the direction of the liquid crystal (LC).

In the definition of liquid crystal (LC) vectors, two angles of $\theta$, $\varphi$ are effective, but since the collision of the radiation wave and the wave propagation direction is in $\theta$ direction, so variations in $\varphi$ are not effective. Therefore, we consider $\varphi$ to be constant with zero value, so the $U_\varphi$ matrix turns into an identity matrix. So, with changes of $\theta$, the molecules of the liquid crystal (LC) change from the vertical in the $\theta$ equal to 0° to the horizontal state in $\theta$ equal to 90°.

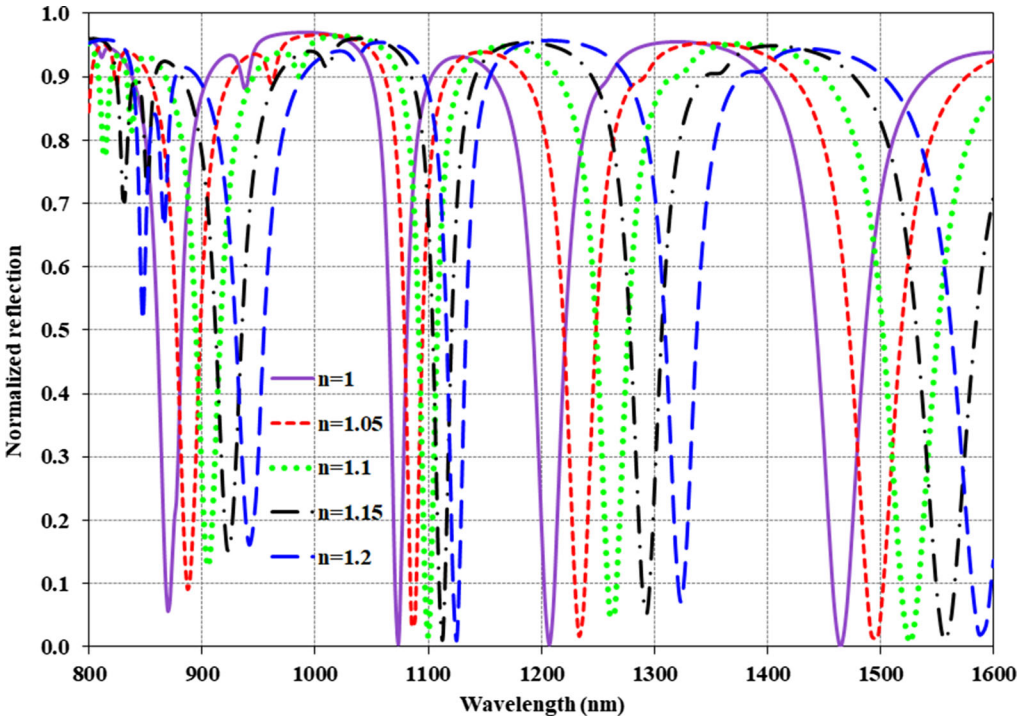


Fig. 6. The normalized reflection of the prototype absorber for various refractive indexes

The results of these variations are presented in Fig. 5 for four different cases. As shown, in general, with these changes from $\theta$ equal to 0° to 90°, the effective permittivity of the structure is decreased, and thus the frequencies increased, or, in other words, the wavelength is decreased. As shown here, we can control resonances and absorption by changing the theta angles. In the first case, when theta and phi are 0°, the matrix has a diagonal form. Also, in this case, as shown in Fig. 5, the resonances have occurred at higher wavelengths and show more distortion at lower wavelengths.

When theta is assumed to be non-zero, we have five non-zero elements in our matrix. Actually, $\varepsilon_{xz}$ and $\varepsilon_{zx}$ are non-zero in this case as mentioned[46] based on Eq. 3. As shown, by increasing theta ($\theta$), the resonances are shifted to the lower wavelengths and we do not have any distortions and when $\theta = 90^{\circ}$, the result is similar to the basic model.

## Using the Prototype Absorber as a Refractive Index Sensing

Given that the plasmonic sensors have a high sensitivity ($S$) due to their small dimensions, to evaluate their performance, some parameters have been introduced such as sensitivity ($S$) and figure of merit (FOM).[47] The sensitivity ($S$) indicates the ratio of output-to-input changes, and by changing the refractive index of the sensor environment to $\Delta n$, the resonance wavelength $\lambda_{SPR}$ changes to $\Delta\lambda$, or $S = \Delta\lambda/\Delta n$. In some cases, the figure of merit (FOM) parameter is defined as $\text{FOM} = \max[\Delta R/R \times \Delta n]$, so that the $R$ is the reflection value at the resonances and $\Delta R$ is the reflection variation due to the small variations of refractive index $\Delta n$.[48,49]

We have covered the nanoparticles with the material under test (MUT) with a total size of 100 nm, to calculate these parameters. It is noteworthy that due to the dependence of the surface plasmon resonance on the adjacent dielectric refractive index, by changing the refractive index of the covered material, the resonance peak in the reflection spectrum shifts. So the proposed structure can be used as a refractive index sensor. We have changed the refractive index ($n$) of the material under test (MUT) from 1 to 1.2 with a step of 0.05.

**Table I. The sensitivity ($S$) and figure of merit (FOM) of the prototype absorber for $n$ = 1 to 1.2**

| | $n$ = 1.05 | $n$ = 1.1 | $n$ = 1.15 | $n$ = 1.2 |
|---|---|---|---|---|
| $\Delta\lambda_1$ | 17.4 | 35.6 | 54.5 | 72 |
| $S_1$ | 348.7 | 355.9 | 363.3 | 359.9 |
| $\text{FOM}_1$ | 239.4 | 146.9 | 101.7 | 63.6 |
| $\Delta\lambda_2$ | 11.7 | 26.7 | 39 | 51.6 |
| $S_2$ | 234.2 | 267 | 260 | 257.85 |
| $\text{FOM}_2$ | 2719.6 | 1671.75 | 1162.5 | 833.1 |
| $\Delta\lambda_3$ | 26.2 | 53.5 | 86.2 | 116.3 |
| $S_3$ | 523.4 | 534.9 | 574.9 | 581.6 |
| $\text{FOM}_3$ | 4317.9 | 2579.7 | 1779.5 | 1347.4 |
| $\Delta\lambda_4$ | 33 | 61.7 | 91.5 | 122.5 |
| $S_4$ | 660.6 | 617.3 | 610.3 | 612.7 |
| $\text{FOM}_4$ | 24560.2 | 16476.1 | 11734.6 | 8995.7 |

**Table II. Comparison of the prototype absorber with previous models based on the figure of merit (FOM), sensitivity (*S*) and structure form**

| | FOM ($RIU^{-1}$) | Sensitivity (nm $RIU^{-1}$) | Structure form |
|---|---|---|---|
| This work | 24560[a]<br>24.4[b] | 660.6 | Quasi-3D absorber |
| Ref[17] | 1090[a] | 700 | Planar absorber |
| Ref[19] | 6838[a] | 1300 | MIM waveguide |
| Ref[26] | 16.54[b] | 1518 | Quasi-3D absorber |
| Ref[31] | 3.04[b] | 260.41 | Planar absorber |
| Ref[37] | 5.78[b] | 1907 | Quasi-3D absorber |
| Ref[47] | – | 2320 | MIM waveguide |
| Ref[49] | $3.2 \times 10^{5}$[a] | 820 | MIM waveguide |
| Ref[50] | 87[a] | 400 | Planar absorber |
| Ref[51] | 37[b] | 4270 | MIM waveguide |

[a]FOM with FOM = max[$\Delta R/R \times \Delta n$]
[b]FOM with FOM = sensitivity(nm/RIU)/FWHM (nm)

Also, we have checked the wavelength shifts and the reflection differences to obtain both sensitivity (*S*) and figure of merit (FOM). In other words, for improving the sensitivity (*S*) it is important to have greater wavelength shift, and for increasing the figure of merit (FOM) both lower reflection and higher difference reflection are important.

Figure 6 shows the reflection of the prototype absorber for various refractive indexes. As shown, we have four resonances, thus we have checked the sensitivity (*S*) and figure of merit (FOM) for all resonances, and the calculated data are compared in Table I. The maximum figure of merit (FOM) for $n = 1.05$ with a value of 24560.2 $RIU^{-1}$ has been obtained. Furthermore, the maximum sensitivity (*S*) has been achieved for the fourth resonance which is about 660.6 nm $RIU^{-1}$.

Moreover, the figure of merit (FOM) can be expressed with another method based on the sensitivity (*S*) and full-width half-maximum (FWHM) while FOM = sensitivity(nm/RIU)/FWHM(nm). Here, the maximum sensitivity (*S*) is 660 nm $RIU^{-1}$ and the full-width half-maximum (FWHM) is 27 nm for the last resonance and, therefore, the figure of merit (FOM) can be calculated as 24.4 $RIU^{-1}$.

## Comparison of the Prototype Absorber with Previous Models

We have compared the prototype structure with various previous models in Table II. We have considered three different types of sensors: quasi-three-dimensional (3D) absorber, planar absorber, and metal-insulator-metal (MIM) waveguide. In fact, in this research, we have used a quasi-three-dimensional (3D) model, and in this absorber, the figure of merit (FOM) is more than other conventional three-dimensional (3D) and planar absorber, and it is comparable with metal-insulator-metal (MIM) structure which is known as the best type of sensor.

Usually, the sensitivity (*S*) and figure of merit (FOM) are known as the two main factors for determining the quality of a sensor. Therefore, we have checked these factors and compared our structure with other similar and non-similar models. Actually, the results show that our structure has a mediocre sensitivity (*S*) while the figure of merit (FOM) factor has been improved drastically in comparison to other models.

Also, it should be noted that we have calculated the figure of merit (FOM) in two methods and compared them with the structures for which each were separately used. The results show that our prototype absorber in the first calculation method has a greater figure of merit (FOM) (24650 ($RIU^{-1}$)) than the other structures that used the same method. As shown in Table II, only the metal-insulator-metal (MIM) waveguide model with Fano resonance has a greater value of figure of merit (FOM) which is about $3.2 \times 10^{5}$ ($RIU^{-1}$).[49] However, the planar absorber[17,50] has a lower figure of merit (FOM) while it has been increased only up to 1090 ($RIU^{-1}$).[17]

In the other case, by the second method, our calculation for the figure of merit (FOM) has been obtained to be 24.4 ($RIU^{-1}$), which is higher than quasi-three-dimensional (3D)[26,37] and planar absorbers.[32] In,[26] a quasi-three-dimensional (3D) absorber has been reported for which the figure of merit (FOM) is about 16.54 ($RIU^{-1}$).

Given that other structures have different fabrication technologies, our proposed structure has a high figure of merit (FOM) of 24.4 ($RIU^{-1}$) compared to similar models with a maximum of 16.54 ($RIU^{-1}$).[26] As a matter of fact, the narrow bandwidth of the prototype absorber increased the figure of merit (FOM), while in[32] the bandwidth is wider than our structure, so the figure of merit (FOM) is reduced to 3.04 ($RIU^{-1}$). In brief, we can emphasize that this absorber has an appropriate

figure of merit (FOM) value in comparison with previous works.

Finally, we have compared the sensitivity ($S$) of the prototyped sensor with other models. As we can see from the Table II, the sensitivity ($S$) of the suggested absorber is 660 (nm $RIU^{-1}$) while this value is about 400 (nm $RIU^{-1}$) for planar structure.[49] However, other metal-insulator-metal (MIM) waveguide[19,47,51] and quasi-three-dimensional (3D) absorbers[26,37] have greater sensitivity ($S$) than our model. The maximum values of sensitivity ($S$) 820 to 4270 (nm $RIU^{-1}$) have been reported for the metal-insulator-metal (MIM) waveguide. The maximum values of sensitivity ($S$) 176 to 700 (nm $RIU^{-1}$) have been obtained for the planar absorbers. In short, given that our proposed absorber is a quasi-3D structure and is more challenging to design than other planer models, it still has a high figure of merit (FOM) and sufficient sensitivity ($S$) when compared to an optical sensor.

## CONCLUSION

In this paper, we have suggested a self-similar perfect absorber with a ziggurat form, which is designed in four steps. In every step, the parasitic elements have been added from large to small with various heights and lengths, and in the last step, the ziggurat form was completed. Also, we have checked the absorption value for all four steps of design, and the results have been compared. First, we checked a single cross element that has only a resonance, and by increasing the number of parasitic elements, the absorption values have increased drastically, while in the last step, we obtained a quad-band perfect absorber. Combining basic absorber structures with quasi-three-dimensional (3D) parasitic elements creates a new way of designing plasmonic sensors, and since height difference is an important factor in the design, the determination of equivalent circuit capacitors will be more complex than planar structures and so is more challenging. Additionally, we have discussed the field intensity at the resonance wavelengths for all four steps of design. We have used liquid crystal (LC) to provide a tunable structure, and the resonances can be controlled by specifying the spatially varying liquid crystal (LC) director orientation instead of a normal substrate. In addition, we have calculated the figure of merit (FOM) and sensitivity ($S$) for the final structure, so that the maximum values have been obtained 24560 $RIU^{-1}$ and 660 nm $RIU^{-1}$, respectively. It should be noted that given that the dimensions of the structure are very small, the manufacturing process must be very accurate. Finally, we have compared our proposed absorber with previous models and as a result, this structure has a much higher figure of merit (FOM) which is a suitable candidate for refractive index sensors.

## REFERENCES


1. T.J. Cui, D.R. Smith, and R. Liu, *Metamaterials* (New York: Springer, 2010).
2. M.K. Hedayati, F. Faupel, and M. Elbahri, *Materials* 7, 1221 (2014).
3. J. Luo, J. Gong, X. Zhang, A. Ji, C. Xie, and T. Zhang, *Optik* 125, 386 (2014).
4. A. Nejati, F.B. Zarrabi, M. Rahimi, and Z. Mansouri, *Optik* 126, 2153 (2015).
5. G. Deng, J. Yang, and Z. Yin, *Appl. Opt.* 56, 2449 (2017).
6. M. Giloan and S. Astilean, *Opt. Commun.* 315, 122 (2014).
7. N.I. Landy, S. Sajuyigbe, J.J. Mock, D.R. Smith, and W.J. Padilla, *Phys. Rev. Lett.* 100, 207402 (2008).
8. V.G. Veselago, *Sov. Phys. Usp* 10, 509 (1968).
9. Z.Y. Liu, Y. Chen, J. Li, T.C. Hung, and J. Li, *Sol. Energy* 86, 1586 (2012).
10. J. Yao, K.T. Tsai, Y. Wang, Z. Liu, G. Bartal, Y.L. Wang, and X. Zhang, *Opt. Express* 17, 22380 (2009).
11. X. Wen, Q. Zhang, J. Chai, L.M. Wong, S. Wang, and Q. Xiong, *Opt. Express* 22, 2989 (2014).
12. S.N. Novin, F.B. Zarrabi, M. Bazgir, S. Heydari, and S. Ebrahimi, *Silicon* 11, 293 (2019).
13. N.H. Anous and D.A. Khalil, *Appl. Opt.* 53, 2515 (2014).
14. N.J. Halas, S. Lal, W.S. Chang, S. Link, and P. Nordlander, *Chem. Rev.* 111, 3913 (2011).
15. K.M. Mayer and J.H. Hafner, *Chem. Rev.* 111, 3828 (2011).
16. E. Hutter and J.H. Fendler, *Adv. Mater.* 16, 1685 (2004).
17. A. Farmani, *JOSA B* 36, 401 (2019).
18. H. Durmaz, Y. Li, and A.E. Cetin, *Sens. Actuators B* 275, 174 (2018).
19. Z. Chen, L. Cui, X. Song, L. Yu, and J. Xiao, *Opt. Commun.* 340, 1 (2015).
20. K.A. Willets and R.P. Van Duyne, *Annu. Rev. Phys. Chem.* 58, 267 (2007).
21. P. Jahangiri, F.B. Zarrabi, M. Naser-Moghadasi, A.S. Arezoomand, and S. Heydari, *Opt. Commun.* 394, 80 (2017).
22. H. Luo and Y.Z. Cheng, *Mod. Phys. Lett. B* 31, 1750231 (2017).
23. A.S. Arezoomand, F.B. Zarrabi, S. Heydari, and N.P. Gandji, *Opt. Commun.* 352, 121 (2015).
24. G. Si, Y. Zhao, E.S.P. Leong, and Y.J. Liu, *Materials* 7, 1296 (2014).
25. P.B. Johnson and R.W. Christy, *Phys. Rev. B* 6, 4370 (1972).
26. Y. Cheng, H. Zhang, X.S. Mao, and R. Gong, *Mater. Lett.* 219, 123 (2018).
27. N.A. Hatab, C.H. Hsueh, A.L. Gaddis, S.T. Retterer, J.H. Li, G. Eres, Z. Zhang, and B. Gu, *Nano Lett.* 10, 4952 (2010).
28. R. Rashiditabar, N. Nozhat, and M.S. Zare, *Plasmonics* 13, 1853 (2018).
29. E. Aslan, E. Aslan, M. Turkmen, and O.G. Saracoglu, *Opt. Mater.* 73, 213 (2017).
30. C. Cao and Y. Cheng, *Appl. Phys. A* 125, 15 (2019).
31. F.J. Jafari, M. Naderi, A. Hatami, F.B. Zarrabi, and A.E.U. Int, *J. Electron. Commun.* 101, 138 (2019).
32. Z. Madadi, K. Abedi, G. Darvish, and M. Khatir, *Optik* 183, 670 (2019).
33. Y. Cheng, X.S. Mao, C. Wu, L. Wu, and R. Gong, *Opt. Mater.* 53, 195 (2016).
34. Y.Q. Ye, Y. Jin, and S. He, *JOSA B* 27, 498 (2010).
35. S. Gottheim, H. Zhang, A.O. Govorov, and N.J. Halas, *ACS Nano* 3, 3284 (2015).
36. A.E. Dorche, S. Abdollahramezani, A. Chizari, and A. Khavasi, *IEEE Photonics Technol. Lett.* 28, 2545 (2016).
37. J. Xu, Z. Zhao, H. Yu, L. Yang, P. Gou, J. Cao, Y. Zou, J. Qian, T. Shi, Q. Ren, and Z. An, *Opt. Express* 24, 25742 (2016).
38. B. Abasahl, C. Santschi, and O.J. Martin, *Acs Photonics* 1, 403 (2014).
39. A. Sakurai, B. Zhao, and Z.M. Zhang, *J. Quant. Spectrosc. Radiat. Transf.* 149, 33 (2014).
40. S. Kang, Z. Qian, V. Rajaram, S.D. Calisgan, A. Alù, and M. Rinaldi, *Adv. Opt. Mater.* 7, 1801236 (2019).
41. S.A. Maier, *Plasmonics: Fundamentals and Applications* (Springer Science & Business Media, 2007).

42. F.B. Zarrabi, R. Hekmati, M. Bazgir, and S. Ebrahimi, *Opt. Quantum Electron.* 50, 452 (2018).
43. F.B. Zarrabi, M. Bazgir, and R. Hekmati, *IEEE Photonics Technol. Lett.* 31, 779 (2019).
44. E. Shokati, N. Granpayeh, and M. Danaeifar, *Appl. Opt.* 56, 3053 (2017).
45. O. Sova, V. Reshetnyak, and T. Galstian, *JOSA A* 34, 424 (2017).
46. Z. Su, J. Yin, and X. Zhao, *Sci. Rep.* 5, 16698 (2015).
47. M.R. Rakhshani and M.A. Mansouri-Birjandi, *Sens. Actuators B* 249, 168 (2017).
48. F. Tavakoli and S. Ebrahimi, *Opt. Quantum Electron.* 51, 185 (2019).
49. Z. Chen and L. Yu, *IEEE Photonics J.* 6, 1 (2014).
50. N. Liu, M. Mesch, T. Weiss, M. Hentschel, and H. Giessen, *Nano Lett.* 10, 2342 (2010).
51. M.R. Rakhshani and M.A. Mansouri-Birjandi, *IEEE Sens. J.* 16, 3041 (2016).